

Thermal interquark potentials for bottomonium using NRQCD from the HAL QCD method

Thomas Spriggs,^{a,*} Chris Allton,^a Timothy Burns^a and Seyong Kim^b

^a*Department of Physics, Swansea University, Swansea SA2 8PP, United Kingdom*

^b*Department of Physics, Sejong University, Seoul 143-747, Korea*

E-mail: t.spriggs.996870@swansea.ac.uk

We report our preliminary progress in the calculation of the interquark potential of bottomonium at non-zero temperature using the HAL QCD method. We use NRQCD correlation functions of non-local mesonic S -wave states to obtain the central potential as a function of temperature. These results have been obtained using our anisotropic 2+1 flavour "Generation 2" FASTSUM ensembles.

*The 38th International Symposium on Lattice Field Theory, LATTICE2021 26th-30th July, 2021
Zoom/Gather@Massachusetts Institute of Technology*

*Speaker

1. Introduction

The interquark potential of quarkonia is one of the first quantities studied in the quest for a deeper understanding of the nature of the strong interaction. Pioneering studies include [1] where the Cornell potential was used to calculate the spectrum of charmonium states using a Quantum Mechanical formalism. In thermal QCD, the temperature dependence of the interquark potential results in quarkonium states melting at different temperatures [2]. These considerations strongly motivate a study of the thermal behaviour of the quarkonia interquark potential.

Heavy quarks interacting via QCD can be approximated using the non-relativistic approach, NRQCD, which allows a significant simplification. NRQCD calculations of bottomonia are typically accurate at the few percent level. In this work we use NRQCD to determine the interquark potential in bottomonia using the HAL QCD approach. Correlation functions of bottomonia operators are studied where the quark and antiquark are non-local, and this allows a proxy for the wavefunction to be calculated. Using this wavefunction in the Schrödinger equation leads to the interquark potential. We find indications of the weakening of the potential as the temperature increases, as expected. This work extends previous studies of the interquark potential by the FASTSUM Collaboration in the charmonium system [3, 4].

2. NRQCD correlation functions and lattice setup

NRQCD is an effective theory with a power counting in the heavy quark velocity, v . In this theory, the heavy quark and antiquark fields decouple and so virtual heavy quark-antiquark loops cannot form. The NRQCD quark propagator is calculated via an initial value problem, rather than via a matrix inversion as is the case for relativistic quarks. NRQCD is particularly amenable for lattice simulations because mesonic correlation functions do not have “backward movers” which complicate the study of QCD mesons.

Our NRQCD formulation incorporates both $O(v^4)$ and the leading spin-dependent corrections. The b -quark mass is tuned by setting the “kinetic” mass (i.e. from the dispersion relation) of the spin-averaged $1S$ states to its experimental value. Full details of our NRQCD setup appear in [5].

All our results were obtained using our FASTSUM $N_f = 2+1$ flavour “Generation 2” ensembles which have the parameters listed in Table 1.

N_τ	16	20	24	28	32	36	40
T [MeV]	352	281	235	201	176	156	141
$N_{\text{configurations}}$	1050	950	1000	1000	1000	500	500

Table 1: An overview of the FASTSUM Generation 2 correlation functions used in this work. Lattice volumes are $(24a_s)^3 \times (N_\tau a_\tau)$ with $a_s = 0.1227(8)\text{fm}$ and $a_\tau = 35.1(2)\text{am}$. For these ensembles with a pion mass of $M_\pi = 384(4)\text{MeV}$, the pseudo-critical temperature $T_{\text{pc}} = 181(1)\text{MeV}$ [6].

3. HAL QCD Method

We follow the HAL QCD time-dependent method to extract the interquark potential [7, 8]. A key quantity for the HAL QCD method is the Nambu Bethe Salpeter (NBS) wave function,

$\psi_i(\mathbf{r}) = \langle 0 | J(\mathbf{r}) | i \rangle$, i.e. the overlap of the non-local mesonic operator $J(\mathbf{r})$ between the vacuum and the bottomonium state $|i\rangle$. The mesonic operator $J(\mathbf{r})$ is defined

$$J_\Gamma(x; \mathbf{r}) = \bar{Q}(x) U(x, x + \mathbf{r}) \Gamma Q(x + \mathbf{r})$$

and thus probes the bottomonium state with a displacement of \mathbf{r} between its two constituent quarks. Γ is a Dirac matrix chosen to have the desired quantum numbers appropriate for either the Υ ($\Gamma = \gamma_i$) or η_b ($\Gamma = \gamma_5$) states, and $U(x, x + \mathbf{r})$ is the gauge connection between x and $x + \mathbf{r}$.

We calculate the zero-momentum correlation function

$$G_\Gamma(\mathbf{r}, \tau) = \sum_{\mathbf{x}} \langle J_\Gamma(\mathbf{x}, \tau; \mathbf{r}) J_\Gamma^\dagger(0; \mathbf{0}) \rangle = \sum_i \frac{\psi_i(\mathbf{r}) \psi_i^*(\mathbf{0})}{2E_i} e^{-E_i \tau} = \sum_i \Psi_i(\mathbf{r}) e^{-E_i \tau}.$$

The sum over states i is the usual spectral representation, and for convenience we've defined

$$\Psi_i(\mathbf{r}) = \frac{\psi_i(\mathbf{r}) \psi_i^*(\mathbf{0})}{2E_i}.$$

Since we are treating the bottom quark nonrelativistically, we can assume that $\Psi_i(\mathbf{r})$ obeys the time independent Schrodinger equation in Euclidean space-time,

$$\left(-\frac{\nabla_r^2}{2\mu} + V_\Gamma(r) \right) \Psi_i(\mathbf{r}) = E_i \Psi_i(\mathbf{r}),$$

where $V_\Gamma(r)$ is the interquark potential for the channel Γ , μ is the reduced mass, and we restrict to S-wave states. Since the correlation function, $G(\tau)$, is a linear combination of $\Psi_i(\mathbf{r})$, we find that it satisfies the Schrödinger equation,

$$\left(-\frac{\nabla_r^2}{2\mu} + V_\Gamma(r) \right) G_\Gamma(\mathbf{r}, \tau) = -\frac{\partial G_\Gamma(\mathbf{r}, \tau)}{\partial \tau}. \quad (1)$$

We use eq(1) to extract the potential, V_Γ from $G_\Gamma(\mathbf{r}, \tau)$. We note that the NRQCD case considered here has a particularly simple form because there are no backward movers. This contrasts with the relativistic case where there are backward movers which need to be considered [3, 4].

We use finite derivatives to approximate the Laplacian and the temporal derivative. Because we consider S-wave states with rotational symmetry, the Laplacian in spherical coordinates can be approximated by

$$\nabla_r^2 f(r) = \frac{\partial^2 f}{\partial r^2} + \frac{2}{r} \frac{\partial f}{\partial r} \approx \left(\frac{f(r + a_s) - 2f(r) + f(r - a_s)}{a_s^2} + \frac{f(r + a_s) - f(r - a_s)}{r a_s} \right). \quad (2)$$

The time derivative is similarly approximated by

$$\frac{\partial f}{\partial \tau} \approx \left(\frac{f(\tau + a_\tau) - f(\tau - a_\tau)}{2a_\tau} \right). \quad (3)$$

Using the leading order terms in the velocity expansion of the interquark potential for S-wave states [9], the central potential can be defined in terms of the potential from the pseudoscalar (i.e. the η_b) and vector (Υ) channels' potentials,

$$V_c(r) = \frac{1}{4} V_{\text{Ps}}(r) + \frac{3}{4} V_{\text{V}}(r). \quad (4)$$

The spin-dependent potential is also accessible to us from these two channels, but is not considered here. Higher order terms in the potential such as the spin-orbit term are also not studied because they require channels with orbital angular momentum.

4. Results

4.1 Derivatives

We begin by separately studying the spatial and temporal derivatives in eq(1). Figure 1 shows the spatial derivative, i.e. the kinetic contribution for the Υ at two indicative temperatures, $T = 141\text{MeV}$ (left) and $T = 352\text{MeV}$ (right). For both temperatures the τ dependence becomes more noticeable at larger r , as does the size of the statistical errors. The increase in noise at larger r is to be expected for point-split lattice correlation functions since points close together are correlated and so fluctuations increase with r .

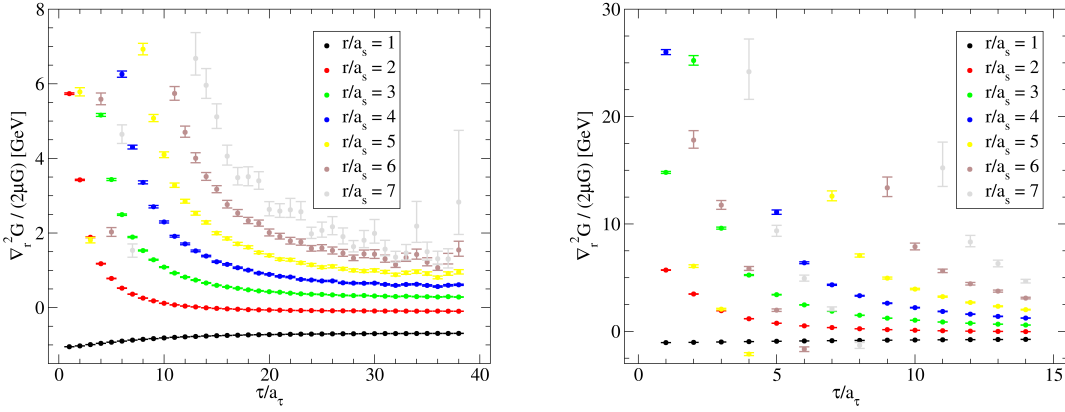


Figure 1: The kinetic (i.e. spatial derivative) contribution to the Υ potential plotted against imaginary time for $T = 141\text{MeV}$ (left) and $T = 352\text{MeV}$ (right). For both temperatures the noise increases with distance, r/a_s . The $T = 352\text{MeV}$ data shows larger variation and the axis scale is adjusted to reflect this.

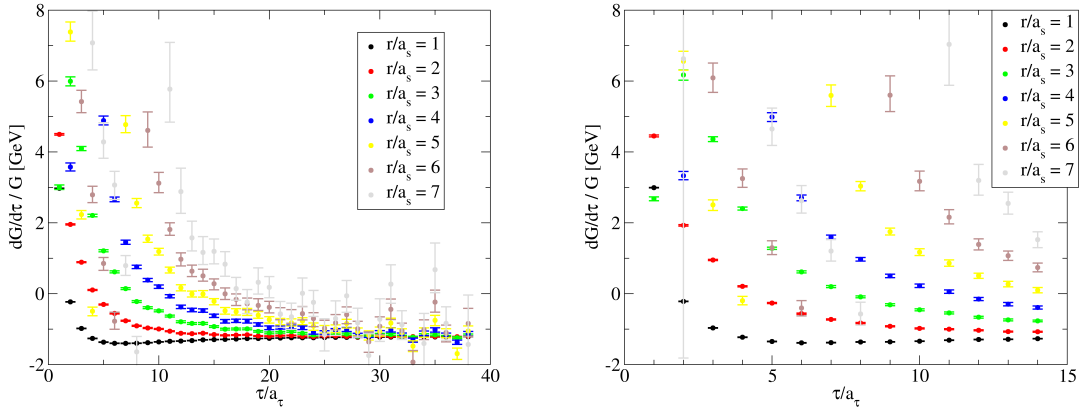


Figure 2: The temporal derivative contribution to the Υ potential plotted against imaginary time for $T = 141\text{MeV}$ (left) and $T = 352\text{MeV}$ (right).

In Fig. 2 we show the temporal derivative term from eq(1) for the same two temperatures. This again shows the variation with r , although this is less than in the spatial derivative case. We

also note that there is a plateau at large τ visible for the $T = 141\text{MeV}$ case. This is to be expected, because at large τ , the time derivative asymptotes to the ground state mass.

Comparing the two derivative from figs.1 & 2, we see that the spatial derivative is numerically larger.

4.2 Potentials for the η_b and Υ Channels

We combine the spatial and temporal derivatives for the η_b and Υ channels in eq(1) to obtain the the potentials for those channels, V_{η_b} and V_{Υ} . The Υ case is plotted in fig.3. Note V_{η_b} and V_{Υ} are explicit functions of τ in the time-dependent HAL QCD method, due to the way these potentials are derived. Ideally, they should be constant functions w.r.t. τ , but as can be seen from fig.3, this is not the case, except at large τ , or for small r . We will investigate this τ -dependency in future work by considering lattice derivatives which are more sophisticated than those in eqs(2) & (3). We note that the results have the smallest systematics for small r values. We obtain our final estimate of the each channel's potential by averaging over a time window as discussed in the next section.

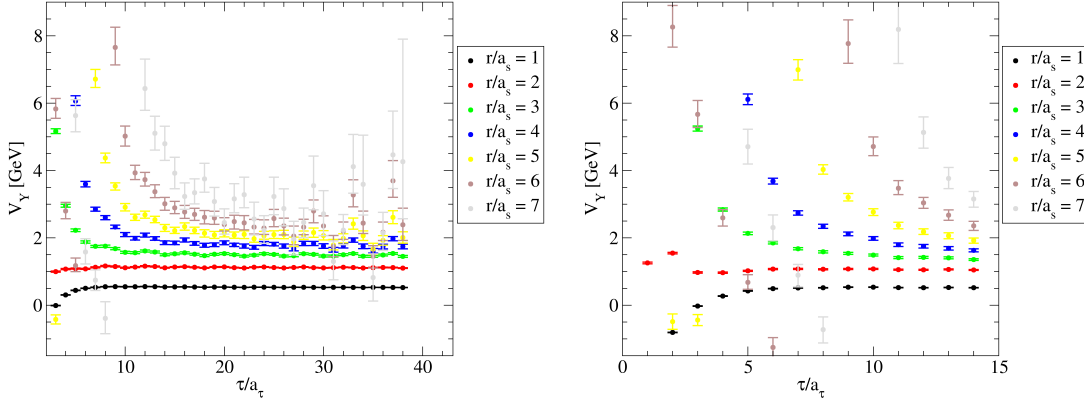


Figure 3: The Υ potential plotted against imaginary time for $T = 141\text{MeV}$ (left) and $T = 352\text{MeV}$ (right).

4.3 Central Potential

We average the potentials for the η_b and Υ channels over the time interval $\tau \in [\tau_1, \tau_2]$ (as discussed below) and then combine them to obtain the central potential, $V_C(r)$ using eq(4). Figure 4 plots $V_C(r)$ for all temperatures studied (see Table 1). Due to the periodic boundary conditions in the spatial direction, there are only 13 distinct lattice points in the spatial direction. However, the noise grows too quickly for points $r > 7a_s$ to be considered.

Our aim is to determine the interquark potential as a function of temperature. In order to disentangle possible systematic effects from thermal effects, we use the *same* time window $[\tau_1, \tau_2]$ for neighbouring temperatures. This ensures that the fitting procedure is identical for both of these temperatures, and so any variation in the potential can be ascribed to a thermal, rather than systematic effect. The data plotted in fig.4 follows this procedure. The points are off-set horizontally for clarity. We see that the potential at large distances $r \gtrsim 0.8\text{fm}$ have large errors and become unstable for the hottest temperatures, but those for distances $r \lesssim 0.8\text{fm}$ have more modest errors and are predictive.

From the plot, we see indications of thermal effects which are best seen in the insert for the two distances $r \approx 0.4$ & 0.5 fm. When considering neighbouring temperatures which share the same time window $[\tau_1, \tau_2]$ we see that there is a clear trend towards a flattening of V_C as T increases. This confirms our expectation that the interquark potential is temperature dependent and becomes weaker with increasing temperature.

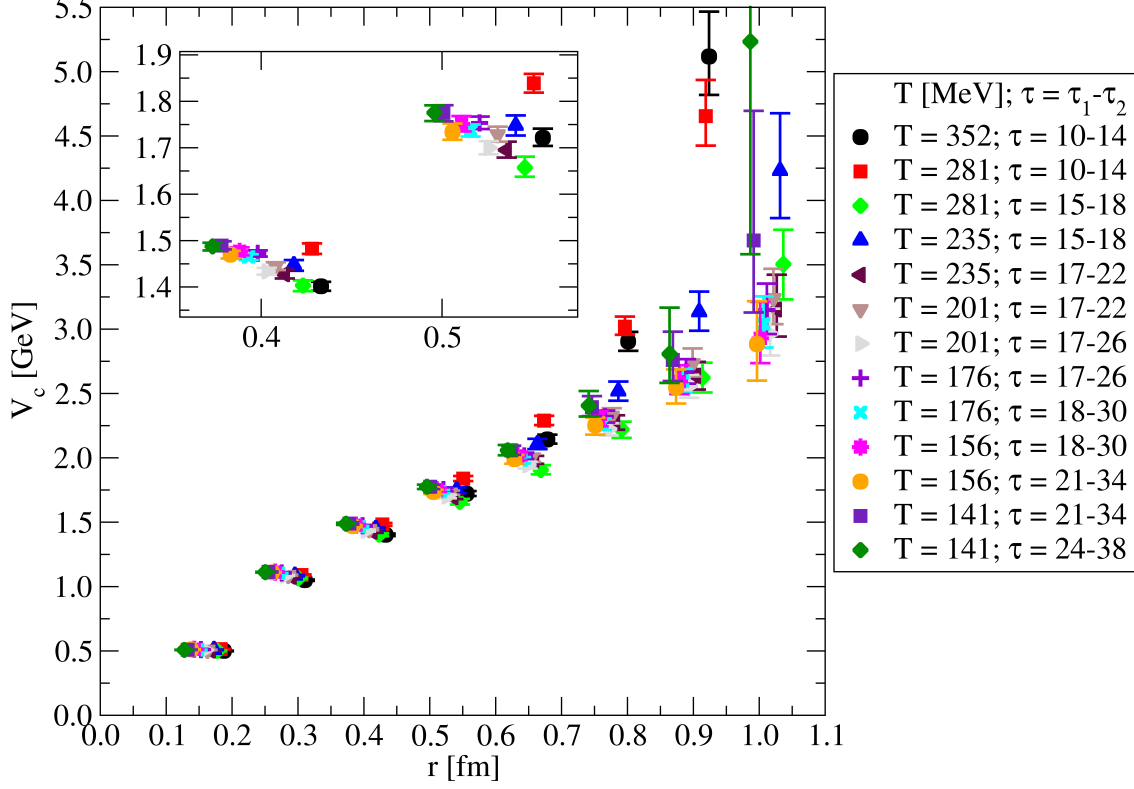


Figure 4: The central interquark potential in the bottomonium system plotted against quark separation r for a range of temperatures. The points are offset horizontally for clarity. The potentials for each temperature are obtained by averaging two time ranges $[\tau_1, \tau_2]$ as indicated in the legend, chosen so that they are identical for neighbouring temperatures. This allows thermal effects to be disentangled from fitting systematics as discussed in the text. The insert shows a closeup of two r values which indicates a thermal effect.

5. Summary

These proceedings present a calculation of the thermal interquark potential in the bottomonium system using the HAL QCD method with NRQCD quarks. Our FASTSUM Collaboration's anisotropic "Generation 2" ensembles were used. We find indications of thermal effects in the central potential, $V_C(r)$, observing the expected flattening of the potential as the temperature increases. Future work will use lattice derivatives which have smaller discretisation errors, and a momentum space approach which will allow us to calculate the potential at all spatial displacements. We will also study higher order terms in the potential.

Acknowledgements

This work is supported by STFC grant ST/T000813/1. SK is supported by the National Research Foundation of Korea under grant NRF-2021R1A2C1092701 funded by the Korean government (MEST). This work used the DiRAC Extreme Scaling service at the University of Edinburgh, operated by the Edinburgh Parallel Computing Centre on behalf of the STFC DiRAC HPC Facility (www.dirac.ac.uk). This equipment was funded by BEIS capital funding via STFC capital grant ST/K000411/1, STFC capital grant ST/H008845/1, and STFC DiRAC Operations grants ST/K005804/1 and ST/K005790/1. DiRAC is part of the National e-Infrastructure. This work was performed using PRACE resources at Cineca via grants 2011040469 and 2012061129. We acknowledge the support of the Supercomputing Wales project, which is part-funded by the European Regional Development Fund (ERDF) via Welsh Government.

References

- [1] E. Eichten, K. Gottfried, T. Kinoshita, K.D. Lane and T.-M. Yan, *Charmonium: The Model*, *Phys. Rev. D* **17** (1978) 3090.
- [2] T. Matsui and H. Satz, *J/ψ Suppression by Quark-Gluon Plasma Formation*, *Phys. Lett. B* **178** (1986) 416.
- [3] P.W.M. Evans, C.R. Allton and J.I. Skullerud, *Ab initio calculation of finite-temperature charmonium potentials*, *Phys. Rev. D* **89** (2014) 071502 [[1303.5331](#)].
- [4] C. Allton, W. Evans, P. Giudice and J.-I. Skullerud, *The Charmonium Potential at Non-Zero Temperature*, [1505.06616](#).
- [5] G. Aarts, C. Allton, T. Harris, S. Kim, M.P. Lombardo, S.M. Ryan et al., *The bottomonium spectrum at finite temperature from $N_f = 2 + 1$ lattice QCD*, *JHEP* **07** (2014) 097 [[1402.6210](#)].
- [6] G. Aarts et al., *Spectral quantities in thermal QCD: a progress report from the FASTSUM collaboration*, *PoS LATTICE2019* (2019) 075 [[1912.09827](#)].
- [7] N. Ishii, S. Aoki and T. Hatsuda, *The Nuclear Force from Lattice QCD*, *Phys. Rev. Lett.* **99** (2007) 022001 [[nucl-th/0611096](#)].
- [8] HAL QCD collaboration, *Hadron-hadron interactions from imaginary-time Nambu-Bethe-Salpeter wave function on the lattice*, *Phys. Lett. B* **712** (2012) 437 [[1203.3642](#)].
- [9] S. Godfrey and N. Isgur, *Mesons in a Relativized Quark Model with Chromodynamics*, *Phys. Rev. D* **32** (1985) 189.